Crystal Structure of Nitromethane up to the Reaction Threshold Pressure

Margherita Citroni,*,†,‡ Fréderic Datchi,§ Roberto Bini,†,‡ Massimo Di Vaira,‡ Philippe Pruzan,§ Bernard Canny,§ and Vincenzo Schettino†,‡

LENS - European Laboratory for Non-Linear Spectroscopy, Universitá di Firenze, via N. Carrara 1, I-50019 Sesto F.no (FI), Italy, [2] Dipartimento di Chimica dell' Universitá di Firenze, via della Lastruccia 3, I-50019 Sesto F.no (FI), Italy, and [3] IMPMC - Physique des Milieux Denses, CNRS, Université Pierre et Marie Curie, 140 rue de Lourmel, 75015 Paris, France

Received: September 5, 2007; In Final Form: October 24, 2007

Angle dispersion X-ray diffraction (AXDX) experiments on nitromethane single crystals and powder were performed at room temperature as a function of pressure up to 19.0 and 27.3 GPa, respectively, in a membrane diamond anvil cell (MDAC). The atomic positions were refined at 1.1, 3.2, 7.6, 11.0, and 15.0 GPa using the single-crystal data, while the equation of state (EOS) was extended up to 27.3 GPa, which is close to the nitromethane decomposition threshold pressure at room temperature in static conditions. The crystal structure was found to be orthorhombic, space group $P2_12_12_1$, with four molecules per unit cell, up to the highest pressure. In contrast, the molecular geometry undergoes an important change consisting of a gradual blocking of the methyl group libration about the C−N bond axis, starting just above the melting pressure and completed only between 7.6 and 11.0 GPa. Above this pressure, the orientation of the methyl group is quasi-eclipsed with respect to the NO bonds. This conformation allows the buildup of networks of strong intermolecular O···H−C interactions mainly in the *bc* and *ac* planes, stabilizing the crystal structure. This structural evolution determines important modifications in the IR and Raman spectra, occurring around 10 GPa. Present measurements of the Raman and IR vibrational spectra as a function of pressure at different temperatures evidence the existence of a kinetic barrier for this internal rearrangement.

1. Introduction

Nitromethane is the simplest nitroalkane and a basic energetic material that decomposes with energy release under shock compression or thermal initiation. Its chemical behavior under dynamic compression has been studied extensively as a model for the behavior of larger explosive materials, but the molecular mechanisms of the detonation process have not yet been fully explained.[1−3] Static pressure does not induce an explosive process, but the knowledge of its effects on nitromethane reactivity could be of help in understanding and modeling the earlier stages of the faster and more extensive reactivity occurring under dynamic stress. Under static compression, crystalline nitromethane chemically transforms into a dark solid or a transparent liquid, both with no Raman signal, depending on the P and T conditions.[4−6] At room temperature, the reaction starts at 28 GPa and its rate increases on increasing pressure or temperature. Many molecular crystals have been shown to react under the effect of a high static pressure, giving rise to new and often more selective reaction paths with respect to those occurring at room pressure in the gas and liquid phases.[7] The reaction mechanisms are dependent on the crystal structure, which in turn is determined by the interplay between the intra- and intermolecular forces. Thus, any insight into the dynamics of a reaction onset in a molecular crystal implies the knowledge of the crystal structure at the reaction pressure.[8]

The crystalline structure of nitromethane at atmospheric pressure, from 4.2 K to the melting point, is orthorhombic, space group $P2_12_12_1$ (D_2^4), with four molecules per unit cell, as obtained by X-ray single-crystal diffraction experiments on nitromethane[9] and neutron powder diffraction experiments on perdeuterated nitromethane.[9] The neutron diffraction data showed that the amplitude of thermal motion of the deuterium atoms, due to the CD_3 group libration around the C−N axis, is rather large even at 4.2 K and its temperature dependence is in perfect agreement with previous inelastic neutron scattering data showing that the barrier to rotation for the methyl group about the C−N bond in the crystal is 118 K (10.2 meV).[10]

Single-crystal X-ray diffraction experiments at room temperature as a function of pressure revealed that nitromethane maintains the same crystalline structure up to 15 GPa.[11−13] Structural refinements were performed at room temperature up to 3.5 GPa.[11] A free rotation of the methyl group was suggested at pressures lower than 3.5 GPa because the H atoms could not be refined below this pressure. At 3.5 GPa, the methyl group was found to be rotated by 44.3° with respect to the staggered conformation of the low-temperature structure. Calculations evidence no phase transitions, in agreement with the diffraction experiments.[14−16] Nevertheless, two DFT calculations predict a rotation of the methyl group from a staggered to an eclipsed conformation, located in the pressure range 10−30 GPa,[15,17] while molecular dynamics simulations report a gradual ordering of the methyl groups, that are almost free to rotate about the C−N bond direction at low pressures and are blocked in an eclipsed conformation at 7 GPa.[16] The pressure-evolution of the Raman spectrum of nitromethane gave results leading to different interpretations. No spectral changes were reported at room temperature up to 11.7 GPa by Cromer et al.[11] However,

* Corresponding author. Phone: +390554572503. Fax: +390554572451. E-mail address: margherita@lens.unifi.it.
† LENS.
‡ Dipartimento di Chimica dell' Universitá di Firenze.
§ IMPMC.

10.1021/jp0771318 CCC: $40.75
Published on Web 01/09/2008

Courtecuisse et al. proposed four phase transitions and two decomposition lines in the *P*, *T* range 0−35 GPa, 300−623 K.[5] The phase transitions were identified by discontinuities or slope breaks in the pressure evolution of the frequencies and bandwidths of the CN, NO_2, and CH_3 stretching modes. The I−II transition, located at 3 ± 0.2 GPa at room temperature, was ascribed to the blocking of the methyl group rotation suggested by Cromer.[11] The II−III transition, located at 7.5 ± 0.5 GPa at room temperature, was interpreted by the authors as a first-order structural transition with a change in the number of molecules per unit cell. A more recent Raman analysis of the lattice modes of CH_3NO_2 and CD_3NO_2 at room temperature up to 45 GPa[18] did not confirm the transition lines of ref 5 but nevertheless revealed important modifications in the spectra above 7 GPa, consisting of a progressive emergence of new peaks in the low-frequency region. These modifications were ascribed by the authors to molecular structural distortions and to the increased intermolecular interactions, not involving a change in the shape of the unit cell or in the number of molecules.

The emergence of new peaks in the vibrational spectra is generally taken as an evidence of a structural tranformation of some kind, and it is therefore necessary to reconcile the X-ray diffraction and the spectroscopic data to fully characterize the pressure evolution of the nitromethane crystal structure, up to the onset of its chemical reaction. To this purpose, in this work, the crystal structure of nitromethane has been investigated by different techniques and in a wide temperature range up to a pressure as close as possible to the reaction threshold. X-ray diffraction experiments allowed us to extend the equation of state up to 27.3 GPa and to refine atomic positions up to 15 GPa. Although the space group ($P2_12_12_1$) and the number of molecules per unit cell (four) are found to be constant in the whole pressure range with no discontinuity in the cell parameters *a*, *b*, and *c*, an important modification is detected in the internal conformation of the molecule. Namely, we observe a gradual blocking of the methyl group libration about the C−N bond axis that is completed between 7.6 and 11 GPa. The transition to the conformationally ordered high-pressure phase is mirrored by the pressure evolution of the IR and Raman spectra around 10 GPa. The pressure evolution of the vibrational spectra probed along different isotherms and on decompression shows that there is a kinetic barrier to this transition.

2. Experimental Methods

For each compression run, a fresh sample of liquid nitromethane (≥99%, from Sigma-Aldrich) was loaded in a membrane diamond anvil cell (MDAC) with no pressure medium. The initial sample dimensions were 50−80 μm in thickness and 100−150 μm in diameter and stainless-steel or rhenium gaskets were used. In the single-crystal diffraction runs, the edge of the rhenium gasket hole was lined with gold in order to achieve a more hydrostatic compression and maintain a good crystal quality on increasing pressure.[19] For the IR measurement, type IIa diamonds were used and a 10-μm-thick layer of nitromethane was deposited on a KBr pellet previously formed in the gasket hole in order to avoid saturation of the absorption bands. After loading, crystallization of the sample in a polycrystalline form was observed at room temperature on increasing pressure to 1.6 GPa. These polycrystalline samples were used in the powder diffraction, Raman, and IR experiments. Single-crystal X-ray diffraction was performed on crystals grown at room temperature in the DAC by melting the powder (by releasing pressure) and then slowly increasing pressure when a single crystalline seed was present in the melt. In all experiments, the pressure was measured by the ruby fluorescence technique.[20]

ADXD experiments were performed at the ID09A beamline of the European Synchrotron Radiation Facility (ESRF) in Grenoble (powder and single-crystal) and at the Institut de Minéralogie et de Physique des Milieux Condensés (IMPMC) in Paris (single-crystal). At the ESRF, a monochromatic X-ray beam with $\lambda = 0.418$ Å was focused onto the sample with a spot diameter of about a 10 μm. A MAR345 image-plate detector was used. Powder diffraction data were collected up to 27.3 GPa in steps of 1−3 GPa. In the single-crystal experiments performed at the ESRF, a DAC with X-ray aperture of 60° was used. A panoramic image was collected every 1−2 GPa up to 19.0 GPa by rotating the DAC about the ω axis by ±30° in a single acquisition with total exposure time ranging from 10 to 30 s. Angle-resolved scans (ω scans) were collected at 7.6 and 11 GPa in angular steps of 3°, and at 15 GPa in steps of 5°, with exposure times of 1−2 s. At IMPMC, an Oxford Diffraction Xcalibur-S diffractometer with a Mo Kα source was used for single-crystal measurements. A DAC with 80° optical aperture was used, and angle-resolved scans were collected at 1.1 and 3.2 GPa with angular steps of 1° and an exposure time of 50 s for each image. A maximum 2θ angle of ±25° was scanned in all of the runs.

The Raman measurements were performed with the 514 nm line of an Ar^+-ion laser, focused on the sample to a spot diameter of about 5 μm. The laser power was kept below 3 mW to prevent photochemical effects. The Raman signal was collected in backscattering geometry and analyzed with a triple monochromator (Jobin-Yvon T64000) equipped with a liquid-N_2-cooled CCD detector. Low temperatures were achieved by keeping the DAC in a liquid He flux cryostat.[21] The temperature was measured with a Chromel-AuFe 0.07% (at 30 K) or Copper-Constantan (at 150 and 250 K) thermocouple welded on the gasket. The spectra were measured with a spectral resolution of 1 cm^{-1} in the range 10−3300 cm^{-1}. The IR spectra were recorded in the mid-IR region 600−5000 cm^{-1} with a spectral resolution of 1 cm^{-1}, with a Bruker IFS-120HR FTIR spectrometer modified to allow measurements with the DAC and in situ measurement of pressure by the ruby fluorescence technique.[22]

3. Results

3.1. X-ray Diffraction. The diffraction images from the powder diffraction experiments were integrated using the Fit2D software.[23] The images revealed large texture effects of the powder sample (i.e., non-constant intensity along the Debye−Sherrer rings) preventing any structural refinement from these data. The observed reflections in the integrated diffraction pattern, in the 2θ range 4−25°, were fitted to pseudo-Voigt functions and could all be indexed by the Dicvol91[24] software assuming an orthorhombic structure, as shown in Figure 1. About 30 reflections of nitromethane were indexed at all pressures (35 at the lowest and 25 at the highest pressure) and were used to calculate the cell parameters, *a*, *b*, and *c*, up to 27.3 GPa, with an error below 0.02%.

In the single-crystal experiments, the cell parameters were derived from the panoramic images collected at the ESRF as a function of pressure up to 19.0 GPa. At each pressure, small portions of the panoramic image containing one or a few peaks were integrated with Fit2D and the peaks were fitted with pseudo-Voigt functions to determine the d-spacings. A fixed region of the image was used at all pressures, corresponding to

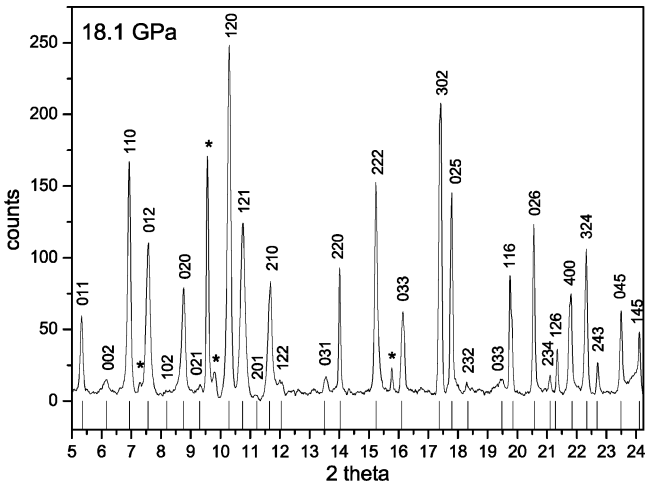

Figure 1. Integrated diffraction pattern of nitromethane powder at 18.1 GPa. Vertical lines: calculated positions (2θ) of the indexed reflections. Stars: ruby reflections (012), (104), (110), and (211) (in order of ascending 2θ).

about one-third of the total image area and containing more than 100 reflections up to 6−7 GPa. The number of reflections decreased at higher pressures because of an intensity decrease: 66 reflections were detected at 14.9 GPa in the same image region, and their number was further reduced to about 20 above 16.9 GPa.

The ω scans at 7.6, 11.0, and 15 GPa collected at ESRF were integrated and analyzed with the software XDS[30] to determine the space group, the cell parameters, and a list of reflections with integrated intensities and standard deviations. The $P2_12_12_1$ space group was confirmed. Above 7.6 GPa, many new reflections appeared. These reflections could be explained by the breaking of the sample into a few crystallites differently oriented (no solution could be found that related the "old" and "new" reflections within the same crystal). Structural refinement above 7.6 GPa was performed using the reflections from the original crystal, which remained the larger set and the most intense, but we checked that the unit cell parameters of the other crystallites were the same as those of the original one. Despite this breaking of the crystal, the single-crystal diffraction spots remained very sharp up to about 15.0 GPa, as shown in Figure 2. At higher pressures the shape of the reflections changed from well-defined spots to patterns more and more similar to a powder-diffraction image, precluding reliable intensity integration of the image.

As shown in the upper panel of Figure 3, there is good agreement between the single crystal and the powder data concerning the values of the cell parameters *a*, *b*, and *c*. Their evolution with pressure does not show any measurable discontinuity or slope discontinuity up to 27.3 GPa. The values of the cell volume as a function of pressure obtained in the powder and in the single-crystal experiments were merged and fitted to the Murnaghan EOS[25]

$$P = \frac{B_0}{B_0'}\left[\left(\frac{V_0}{V}\right)^{B_0'} - 1\right]$$

where V_0 is cell volume at $P = 0$, B_0 is the bulk modulus, and B_0' its first derivative with pressure. We chose this EOS form to compare with results from previous studies.[11,13] With the value of V_0 fixed at 292.7 Å^3, the value reported in references 11 and 13, the resulting B_0 and B_0' values are $B_0 = 8.3 \pm 0.2$ GPa and $B_0' = 5.9 \pm 0.1$ (reduced $\chi^2 = 0.151$) in perfect agreement with the literature data, that were limited to 15 GPa. Relaxing V_0, the fit gave $V_0 = 290 \pm 7$ Å^3, $B_0 = 9.25 \pm 1.9$ GPa and $B_0' = 5.7 \pm 0.2$ (reduced $\chi^2 = 0.153$). The curve obtained with this latter fit is reported in the lower panel of Figure 3. Using the Vinet EOS model,[26] which is a more realistic model at large compression,[27−29] and by fixing $V_0 = 292.7$ Å^3, we obtained $B_0 = 8.3 \pm 0.3$ GPa and $B_0' = 7.4 \pm 0.3$ for pressures above 15 GPa.

The single-crystal data were used for the refinement of the atomic positions. The structure was solved and refined with the suite SHELX-97.[31] Structure solving and refinement were also performed with Sir92[32] and Crystals,[33] respectively, that gave consistent results. We report the results obtained from the analysis performed with SHELX-97. The relevant parameters of the refinement procedure are reported in Table 1, and the fractional atomic coordinates and the bond lengths and angles are reported in Tables 2 and 3, respectively. For each non-H atom in the asymmetric unit CH_3NO_2, the three Cartesian coordinates and the isotropic thermal parameter U (Å^2) were refined. After structure solving and preliminary refinement of the non-H atoms, the positions of the H atoms were found by Fourier difference analysis and then optimized with the constraint of a rigid idealized methyl group, with C−H bond distances fixed at 0.96 Å and HĈH and CN̂H angles fixed at 109.47°. The idealized and rigid methyl group was left free to rotate about the C−N bond axis. The U values of the H atoms were constrained at 1.5 times the U value of the C atom. At 1.1, 3.2, and 7.6 GPa, the Fourier difference analysis indicated the existence of six to four maxima (more evident at lower pressures) that could be identified as H atoms bonded to the C atom. The methyl group was modeled as being distributed between two orientations about the C−N bond direction, having complementary population parameters whose values were refined. The relative population of one methyl fraction, with the same eclipsed orientation with respect to the NO_2 plane as reported by Cromer at 3.5 GPa,[11] was found to be about 52% at 1.1 GPa and to increase gradually with increasing pressure. The alternative orientation of the methyl group is staggered with respect to the NO_2 plane and similar to that found by Trevino at low temperature and room pressure.[9] Consistent with the results of the Fourier difference analysis, at 1.1 and 3.2 GPa, refinement with a unique methyl group orientation gave high GofF values and large thermal parameters for the H atoms if unrestrained. At 7.6 GPa, models with a unique or a 2-fold disordered methyl orientation yielded similar values of R and GofF with prevailing eclipsed form. At 11.0 and 15.0 GPa, it was impossible to refine two methyl orientations because either the population of the staggered form was zeroed or the two fractions, with comparable populations, merged to the eclipsed orientation. Refinement with 3 H positions yielded the eclipsed conformation, and the Fourier difference analysis did not reveal any extra H fraction to be included.

3.2. Pressure Evolution of the Vibrational Spectra. Raman spectra were recorded along isothermal compressions at 30, 150, and 250 K, while FTIR spectra were measured at room-temperature both on increasing and on releasing pressure. For each isothermal run, a new freshly loaded sample was used. Above 25 GPa, the use of laser light for the measurement of the Raman spectra, even limiting the power to few milliwatts, caused the transformation of nitromethane into a transparent product with no Raman signal. The IR spectra could be measured up to 32.0 GPa, and above this pressure a spontaneous chemical transformation was also observed. This difference in the threshold pressure for chemical transformation is to ascribe

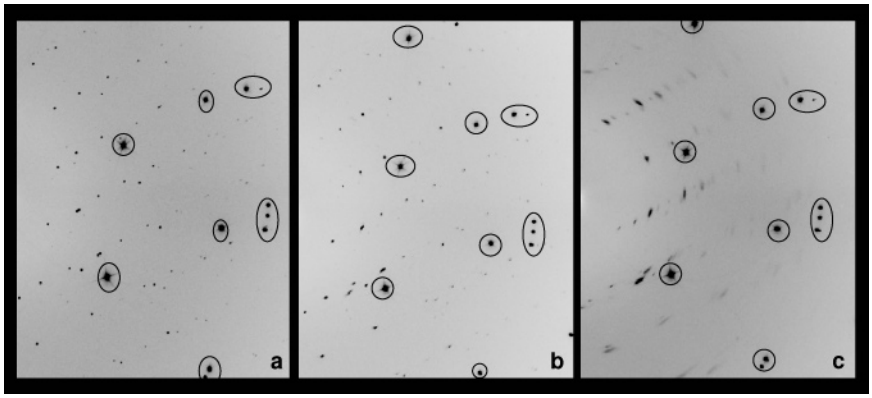

Figure 2. Detail of the MAR3450 images collected in the panoramic acquisitions over 60° of rotation of the DAC around the ω axis (see text). Circled reflections are due to the diamond anvils. (a) 5.06 GPa; (b) 12.5 GPa; (c) 19.0 GPa.

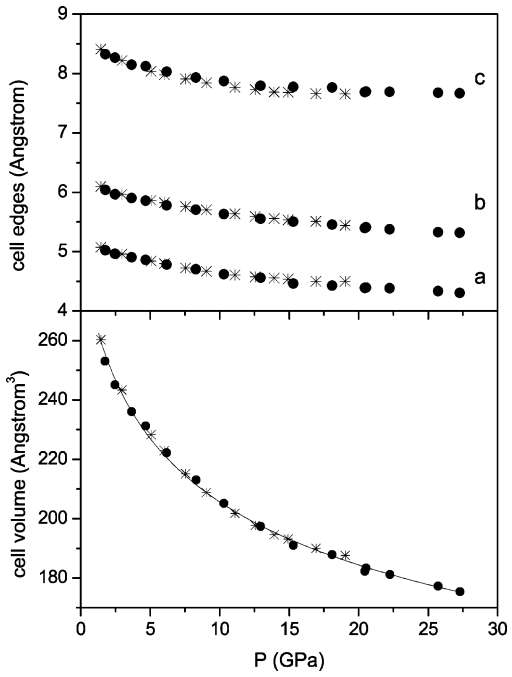

Figure 3. Cell parameters (upper panel) and cell volume (lower panel) of nitromethane as a function of pressure. Stars: single-crystal diffraction data. Circles: powder diffraction data. Line: fit to the Murnaghan EOS (see text).

TABLE 1: Refinement Parameters

	1.1 GPa	3.2 GPa	7.6 GPa[a]	7.6 GPa	11.0 GPa	15.0 GPa
refl. measured	840	993	475	475	445	408
independent refl.	223	346	323	323	304	277
$F_0 > 4\sigma(F_0)$	180	260	249	249	253	196
R-factor	0.0859	0.0991	0.1312	0.1306	0.1376	0.158
weighted *R*-factor	0.2410	0.2571	0.3702	0.3724	0.4228	0.4991
GofF	1.192	1.266	1.413	1.418	1.655	1.677
refined parameters	20	20	20	18	18	18

[a] Refinement made with two methyl fractions at 7.6 GPa (see text). Refinement was performed on F^2 using all of the measured reflections, with a weigthing scheme: $w = 1/(\sigma^2(F_o^2) + (aP)^2 + bP)$; where $P = (\mathrm{Max}(F_o^2,0) + 2F_c^2)/3$. The coefficients a and b could only be refined at 1.1 GPa (a =0.1554 and b =0.18) and at 3.2 GPa (a =0.0476 and b =1.98), at the other pressures they were fixed at a =0.2 and b =0.

to the different irradiation conditions: in the Raman measurements the sample was irradiated for many hours with about 3 mW at 514 nm, while in the IR experiments the sample was irradiated only for few seconds at each pressure step to excite the ruby fluorescence with a power of about 0.1 mW at 532 nm. The IR experiments can thus be considered almost free from laser irradiation effects. The IR data collection on releasing pressure was performed on samples compressed up to 18 GPa.

TABLE 2: Lattice Parameters and Atomic Coordinates Obtained from the Refinement of the Single-Crystal Diffraction Data

	1.1 GPa	3.2 GPa	7.6 GPa[a]	7.6 GPa	11.0 GPa	15.0 GPa
a	5.087 (2)	4.9069 (7)	4.718 (2)	4.718 (2)	4.607 (4)	4.540 (6)
b	6.1160 (6)	5.9055 (5)	5.731 (1)	5.731 (1)	5.636 (3)	5.534 (4)
c	8.435 (3)	8.1422 (9)	7.851 (3)	7.851 (3)	7.771 (5)	7.687 (5)
V	262.4 (2)	235.94 (8)	212.3 (2)	212.3 (2)	203.2 (4)	193.1 (5)
N						
x	0.8580 (4)	0.855 (2)	0.862 (2)	0.862 (2)	0.867 (2)	0.855 (3)
y	0.5820 (5)	0.587 (1)	0.5826 (9)	0.5825 (9)	0.583 (1)	0.583 (2)
z	0.6194 (2)	0.617 (1)	0.6093 (7)	0.6091 (7)	0.6050 (9)	0.605 (1)
U	0.0346 (4)	0.025 (2)	0.022 (2)	0.021 (2)	0.018 (2)	0.018 (3)
O1						
x	0.8862 (4)	0.894 (2)	0.907 (2)	0.907 (2)	0.918 (2)	0.917 (3)
y	0.7156 (5)	0.713 (1)	0.713 (1)	0.713 (1)	0.709 (1)	0.704 (2)
z	0.7267 (2)	0.731 (1)	0.7333 (7)	0.7332 (7)	0.733 (1)	0.732 (1)
U	0.0597 (5)	0.043 (2)	0.040 (2)	0.040 (2)	0.033 (2)	0.032 (3)
O2						
x	1.0186 (3)	1.018 (2)	1.019 (2)	1.019 (2)	1.0111 (2)	1.009 (3)
y	0.5668 (4)	0.568 (1)	0.565 (1)	0.564 (1)	0.566 (1)	0.565 (2)
z	0.5111 (2)	0.503 (1)	0.4904 (7)	0.4907 (7)	0.481 (1)	0.480 (2)
U	0.0513 (5)	0.0392 (19)	0.0365 (19)	0.037 (2)	0.034 (2)	0.034 (3)
C						
x	0.6249 (5)	0.613 (2)	0.596 (2)	0.594 (3)	0.585 (3)	0.569 (4)
y	0.4427 (7)	0.448 (2)	0.449 (1)	0.448 (1)	0.451 (2)	0.453 (3)
z	0.6170 (2)	0.616 (1)	0.616 (1)	0.614 (1)	0.612 (1)	0.609 (2)
U	0.0411 (6)	0.036 (2)	0.033 (2)	0.033 (2)	0.029 (3)	0.032 (4)
H1						
x	0.671	0.661	0.639	0.634	0.621	0.602
y	0.299	0.294	0.286	0.291	0.289	0.285
z	0.652	0.643	0.620	0.646	0.644	0.632
H2						
x	0.494	0.486	0.491	0.468	0.460	0.446
y	0.503	0.504	0.492	0.517	0.524	0.520
z	0.686	0.696	0.714	0.696	0.696	0.699
H3						
x	0.557	0.531	0.486	0.507	0.495	0.472
y	0.435	0.452	0.481	0.451	0.455	0.470
z	0.511	0.509	0.516	0.505	0.500	0.499
H4						
x	0.666	0.638	0.599			
y	0.307	0.323	0.348			
z	0.566	0.541	0.712			
H5						
x	0.568	0.580	0.439			
y	0.415	0.390	0.554			
z	0.724	0.725	0.624			
H6						
x	0.487	0.460	0.578			
y	0.515	0.537	0.357			
z	0.560	0.582	0.515			
relative pop. H4−H6	0.485	0.267	0.228			

[a] Refinement made with two methyl fractions at 7.6 GPa (see text).

TABLE 3: Bond Lenghts (Å) and Angles (Degrees) Obtained from the Refinement of the Single-Crystal Diffraction Data

P (GPa)	C−N	N−O1	N−O2	O1N̂O2	CN̂O1	CN̂O2
1.1	1.460 (4)	1.228 (3)	1.229 (2)	121.4 (2)	119.6 (2)	119.1 (2)
3.2	1.45 (1)	1.21 (1)	1.23 (1)	122.3 (9)	118.9 (9)	118.8 (8)
7.6[a]	1.48 (1)	1.253 (7)	1.200 (9)	124.1 (8)	115.5 (7)	120.4 (7)
7.6	1.48 (1)	1.254 (7)	1.20 (1)	124.2 (8)	115.6 (7)	120.2 (7)
11.0	1.50 (1)	1.24 (1)	1.17 (1)	127 (1)	114.8 (8)	118.4 (8)
15.0	1.49 (2)	1.22 (2)	1.19 (2)	124 (1)	117 (1)	119 (1)

[a] Refinement made with two methyl fractions at 7.6 GPa (see text).

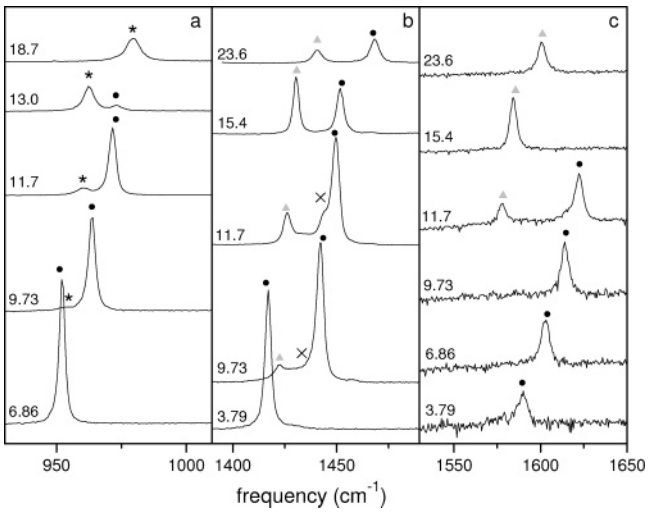

Figure 4. Pressure evolution of selected parts of the Raman spectrum at 250 K. Above each spectrum the pressure at which it was recorded is marked (GPa). (a) CN stretching mode ν_{11}. (b) NO_2 symmetric stretching mode ν_7, CH_3 deformation modes ν_5 and ν_6. (c) NO_2 asymmetric stretching mode ν_4.

The molecular symmetry of nitromethane is C_s so that its 15 internal modes of vibration (9 A′ and 6 A″) are all IR and Raman active. In the crystal (site group C_1, factor group D_2) each internal mode gives rise to four Davydov components with symmetries $A + B_1 + B_2 + B_3$. All of the components are Raman active, but only those with B_1, B_2, and B_3 symmetry are IR active. Twenty-one lattice modes are present, distributed among the symmetry species as $6A + 5B_1 + 5B_2 + 5B_3$. The frequency of the torsional mode of the methyl group about the C−N axis falls in the lattice phonon region, at about 50 cm^{-1}; all of the other internal modes are clearly separated in frequency from the lattice modes. The assignments are given on the basis of the data reported in refs 34 (Raman) and 35 (IR).

Close to ambient temperature, both Raman and IR spectra show remarkable changes in the internal mode region from 8 GPa up to about 14 GPa, apparently confirming the results reported in ref 5 and interpreted by the authors as evidence of several phase transitions.

At 30 K, the frequency evolution with pressure of the lattice and internal Raman modes does not show any discontinuity or derivative discontinuity. A similar frequency evolution with pressure is observed in the isothermal compression at 150 K, but changes in the relative intensities of some crystal modes take place between 11.5 and 15.0 GPa. This effect is definitely more pronounced in the isothermal run at 250 K in the pressure range 9.7−13.0 GPa (Figure 4). In this pressure range, we observe for several modes the appearance of new low-frequency components that intensify with rising pressure, while the high-frequency components weaken and, in some cases, disappear

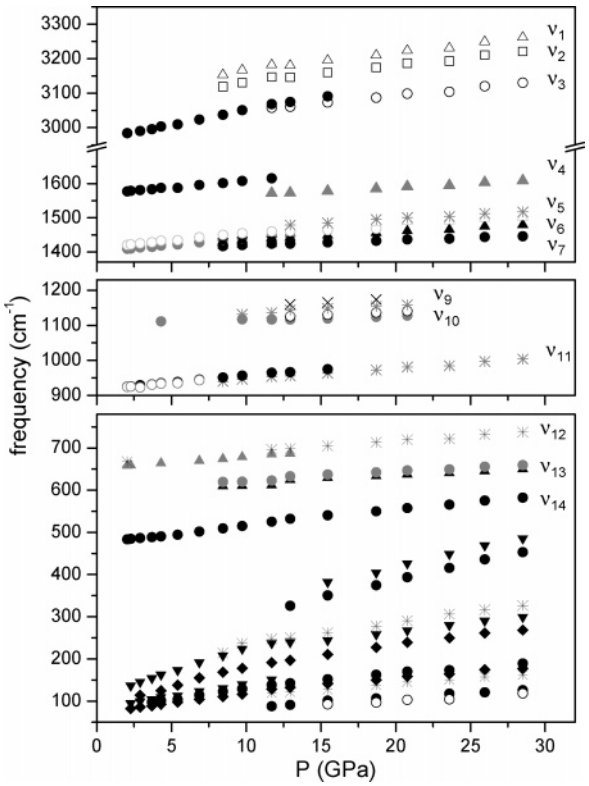

Figure 5. Pressure evolution of the frequencies of the observed Raman modes at 250 K.

upon compression. The most striking change is reported in panel c of Figure 4, showing the region of the NO_2 asymmetric stretching mode. At 11.7 GPa, a new component suddenly grows about 50 cm^{-1} below the other component that, in turn, is not observable anymore at 13.0 GPa. The appearance and growth of this band is also observed at 150 K, and a similar behavior is observed for the ν_{11} and ν_7 modes (panels a and b of Figure 4, respectively). Small slope changes are detectable in the frequency evolution of some lattice and internal modes, as can be seen in Figure 5. Polarization effects, due to a change in the orientation of the crystallites probed by the laser beam, cannot be considered responsible for this observation because the same behavior was observed in different samples and in the IR experiments, discussed in the following, where the incident beam is depolarized and all of the powdered sample is probed simultaneously.

The IR spectra closely mirror the Raman observations because new absorption bands start to be detected at about 8−9 GPa (Figure 6). A remarkable observation is the strong intensification of the CH stretching modes on increasing pressure: the asymmetric stretching modes ν_2 and ν_3 are very weak at low pressures and become clearly detectable only above 6 GPa, but a steep increase of their intensity takes place at about 9 GPa, where a decrease of the slopes of the frequency versus pressure curves of several modes is also observed (Figure 7). From 15.0 to 32.0 GPa, the frequencies of all of the modes increase continuously and without slope changes and their relative intensities remain constant. The IR spectrum was also monitored on releasing pressure from 18 GPa on samples that were not pressurized above this pressure. The frequencies of all of the modes are reversible with pressure. However, the relative intensities are not reversible and the same intensity patterns as those in the high-pressure spectra are maintained at least down to 4.7 GPa. Namely, the new component of the ν_4 and ν_{11} modes and the new strong component of the ν_7 mode, that clearly

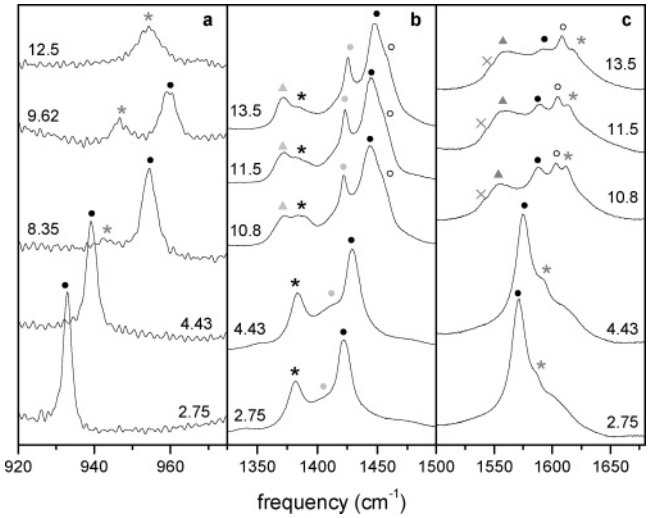

Figure 6. Pressure evolution of selected parts of the IR spectrum at 298 K. (a) CN stretching mode ν_{11}. (b) CH_3 deformation mode ν_8 and NO_2 symmetric stretching mode ν_7. (c) NO_2 asymmetric stretching mode ν_4.

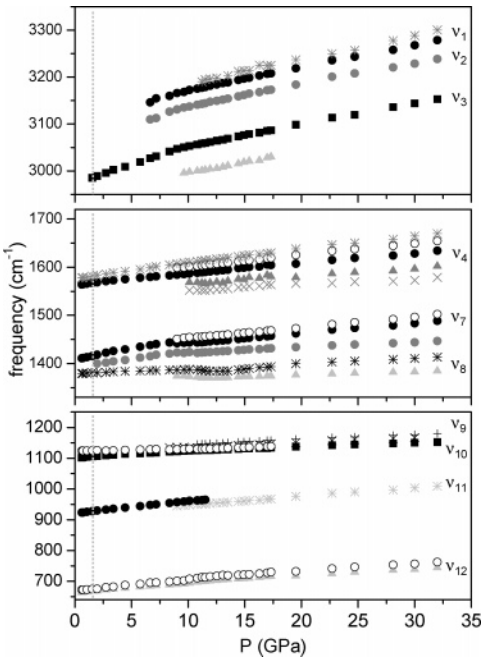

Figure 7. Pressure evolution of the frequencies of the observed IR modes of nitromethane at 298 K upon compression. The dotted line indicates the pressure at which solidification occurred (2.0 GPa).

appeared at 9.0 GPa and whose intensity increased strongly upon compression, do not weaken at all during decompression. However, upon decreasing pressure below 3 GPa, or heating the sample at 50 °C for a few minutes at 5−6 GPa, the IR spectrum suddenly recovers the low pressure intensity distribution (Figure 8).

4. Discussion

The single-crystal and powder X-ray diffraction data show that the $P2_12_12_1$ structure of nitromethane with four molecules per unit cell, found in previous studies to be stable up to 15 GPa,[11−13] is maintained at room temperature from the melting up to 27.3 GPa, a pressure close to the threshold of a slow chemical reaction.[5,6] The values of the cell parameters *a*, *b*, and *c* reduce smoothly on increasing pressure with no discontinuities or slope breaks. We thus extended the equation of state up to

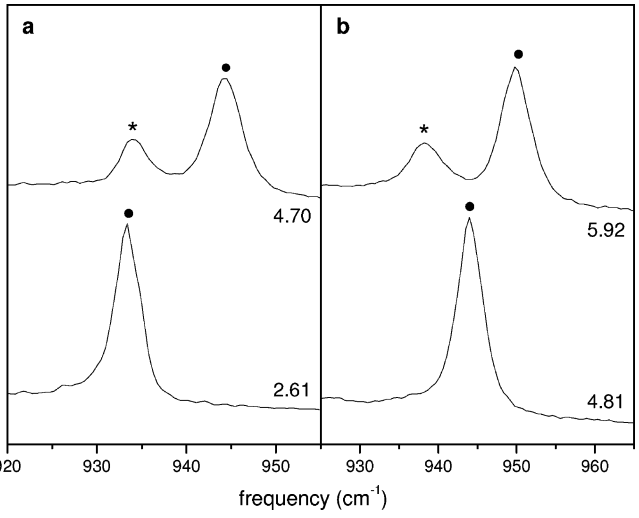

Figure 8. Pressure evolution, on decompression, of the IR spectrum in the region of the CN stretching mode ν_{11}. The pressure values at which the spectra were measured are indicated in the figure. Panel a: decompression at room temperature. Panel b: spectra measured before (upper trace) and after (lower trace) heating the sample at 50°.

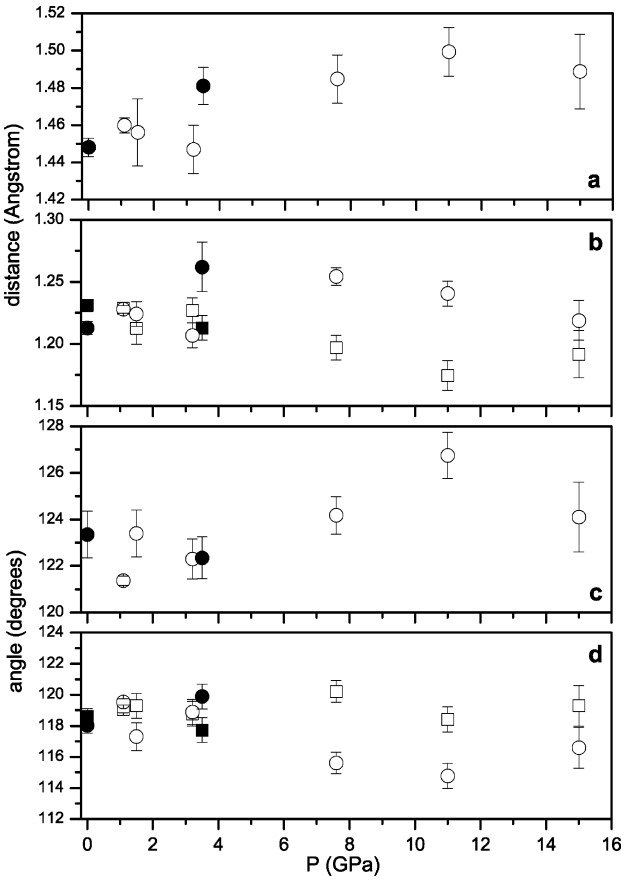

Figure 9. Pressure-evolution of intramolecular bond lengths and angles. Full symbols: low-temperature (−45 °C) data from ref 9 ($P = 0$), and room-temperature data from ref 11 ($P = 3.5$ GPa). Empty symbols: this work. (a) Pressure-evolution of the C−N bond length. (b) Pressure-evolution of the two N−O bond lengths. Circles: N−O1 bond length. Squares: N−O2 bond length. (c) Pressure-evolution of the $\hat{ONO}$ angle. (d) Pressure-evolution of the $\hat{CNO}$ angles. Circles: $\hat{CNO}1$. Squares: $\hat{CNO}2$.

the chemical instability boundary, with B_0, B_0' and V_0 values that are in agreement with those obtained previously at lower pressures. From the refinement of the diffraction data, no clear discontinuity is found in the pressure evolution of any of the

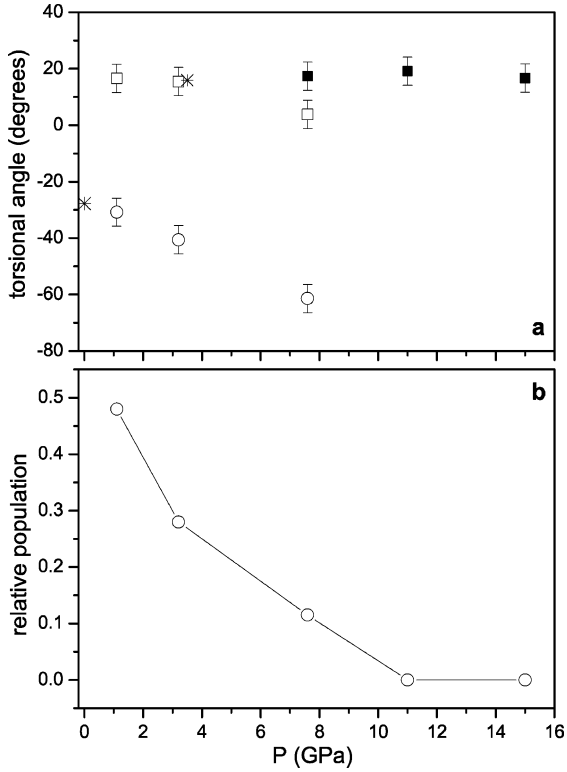

Figure 10. Panel a: pressure-evolution of the minimum (in absolute value) O1−N−C−H torsional angle for each refined model. Stars: low-temperature (−45 °C) data from ref 9 ($P = 0$), and room-temperature data from ref 11 ($P = 3.5$ GPa). Empty symbols: results of the refinements performed on models containing two methyl fractions; circles: conformation with the smallest population (staggered); squares: conformation with the largest population (eclipsed). Full symbols: results of the refinements performed on models containing a unique methyl orientation. Panel b: pressure-evolution of the relative population of the staggered conformation. At 7.6 GPa, the relative population of the staggered conformation was estimated as 0.115, that is the average of 0.23 (the value obtained by refinement with two methyl fractions), and zero (virtual value when refining with one methyl orientation, where the molecule assumed the eclipsed conformation).

other structural parameters, as mentioned already for *a*, *b*, and *c*. The C−N bond length and the ONÔ angle increase slightly up to 11.0 GPa. The bond lengths and angles involving the two oxygen atoms become quite different from each other at 7.6 GPa (panels *b* and *d* of Figure 9), due to the increased and unequivalent intermolecular interactions. Nonetheless, there is a strong modification in the molecular geometry upon raising pressure up to 11 GPa, consisting of a gradual blocking of the methyl group in a quasi-eclipsed position with respect to the NO_2 plane: from the refinement it is clear that two different intra- and intermolecular arrangements of the nitromethane molecules are possible in the crystal, and we will call them phase I and phase II.

Phase I is characterized by orientational disorder due to the methyl group libration about the C−N bond axis. The structural refinement suggests that there are two minima, or two limiting positions, for this coordinate corresponding to an eclipsed and a staggered conformation with respect to the NO_2 plane. These are the same conformations as found, respectively, by Cromer at 3.5 GPa[11] and by Trevino at low-temperature and room pressure,[9] as shown in the upper panel of Figure 10. In the lower panel of the same figure, the relative population at room temperature of the staggered conformation is reported as a function of pressure: it is 50% at a pressure just above the melting point and decreases gradually to become zero at 11.0

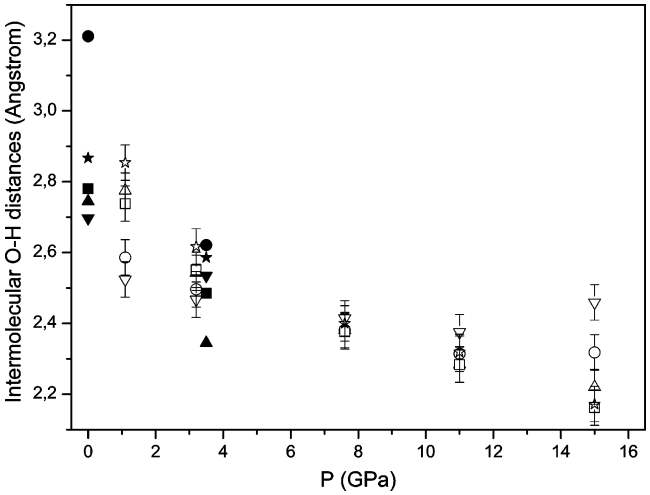

Figure 11. Pressure evolution of five out of the six shortest intermolecular O···H distances. Full symbols: low-temperature (−45 °C) data from ref 9 ($P = 0$), and room-temperature data from ref 11 ($P = 3.5$ GPa). Empty symbols: this work. Circles: O1(B)···H3-(A). Up triangles: O2(A)···H2(B). Down triangles: O1(C)···H1(B). Squares: O2(C)···H1(A). The letters A, B, and C indicate symmetry-related molecules in the unit cell labeled as shown in Figure 12. Stars: O2···H3 distances between nearest molecules belonging to adjacent unit cells along *a*.

GPa. Phase II is the high-pressure crystalline phase of nitromethane containing only molecules with the eclipsed conformation. In interpreting the results of neutron powder diffraction experiments on CD_3NO_2 up to 5.5 GPa, Von Dreele et al.[13] used a similar method to model the D atoms disorder. By refining the relative populations of two CD_3 group fractions free to rotate about the C−N bond direction, they found a 50−50% population at 0.6 GPa and 20−80% population at 5.5 GPa, in agreement with the present results. Our results are also in optimal agreement with the already mentioned MD predictions of Sorescu et al.,[16] where the torsional angle at 7 GPa differs by about 50° from the low-pressure equilibrium value. The authors found that the high-pressure structure is mainly stabilized by O···H interactions.

Indeed, following the molecular conformation change, a network of O···H−C hydrogen bonds builds up, whose strength increases with increasing pressure (Figure 11). At high pressure, the shortest O···H distance inside the unit cell occurs between O2 of molecule C and H1 of molecule A (Figure 12). This interaction is directed mainly along the *b* axis and connects in a zigzag pattern the molecules lined up along the *a* axis with alternating NO_2 and CH_3 groups. An O···H interaction of similar strength and mainly directed along the *a* axis builds up between O2 and H3 of molecules belonging to adjacent unit cells. At the same time, chains of A and B molecules are formed along the *c* axis with a double O···H interaction (O2(A)−H2(B) and O1(B)−H3(A)). Moreover, the O2 atom of molecule C, that is involved in the shortest intermolecular interaction mentioned above, also has a strong interaction with the H2 atom of molecule D, thus forming a bifurcated bond. This last interaction is exactly equal to O1(B)−H3(A). All of these interactions can indeed be classified as H-bonds because the distances between the proton donor and the proton acceptor are 2.95, 2.80, 3.02, and 2.88 Å, respectively, and the OĤC angles are 139.9°, 121.9°, 129.8° ,and 124°, respectively (180° being the optimum OĤC angle that would allow the maximum H-bond covalent character). Alternatively, the O1(C)−H1(B), that is the shortest intermolecular interaction at low pressure and has its largest component along *a*, weakens above 11 GPa so that the main

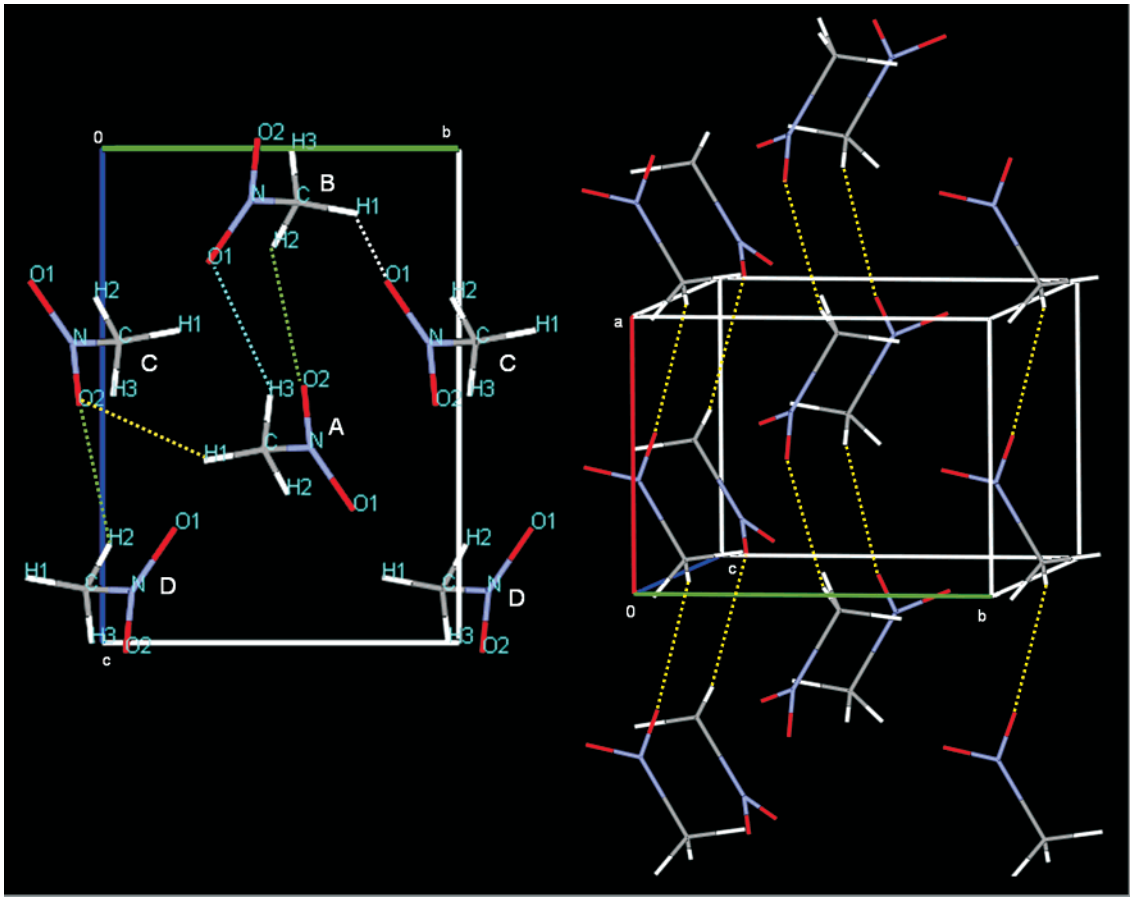

Figure 12. Two views of the molecular arrangement in the crystal at 15.0 GPa as obtained by structure refinement from the single-crystal data. In addition to the intramolecular bonds, in the left panel the shortest intermolecular O···H distances inside the unit cell are shown. The symmetry-related molecules are indicated with different uppercase letters. The O2(C)···H1(A) distance is 2.16 Å, the O1(B)···H3(A) distance is 2.32 Å, the O2(A)···H2(B) and O2(C)···H2(D) distances are 2.22 Å, and the O1(C)···H1(B) distance is 2.46 Å. In the right panel, the O2···H3 distances between nearest molecules belonging to adjacent unit cells, and mainly directed along *a*, are shown. This distance is 2.17 Å.

intermolecular interactions at 15 GPa are in the *bc* and *ac* planes. The buildup of the H-bonds is also evidenced by the strong intensification of the C−H stretching modes in the IR spectra between 6 and 9 GPa. This network stabilizes the high-pressure crystalline structure and fixes the methyl group to form II until the reaction threshold pressure.

The important and continuous changes taking place in both Raman and IR spectra between 8 and 13 GPa can then be viewed as a consequence of the complex response of the molecular framework to the increasing intermolecular interaction driven by the O···H−C interactions. In fact, all of the intensity changes occur below 15.0 GPa. Phases I and II of nitromethane have different IR and Raman spectra and slightly different compressibilities: phase II is less compressible than phase I, as revealed by the different pressure-evolution of the spectra (Figures 5 and 7). Phase II remains metastable on releasing pressure. Only by heating the sample at least at 50 °C or lowering the pressure below 3 GPa is phase I recovered, as revealed by the IR spectra (Figure 8). This indicates the existence of a kinetic barrier in breaking the intermolecular network and restoring the staggered low-pressure conformation, coexisting with the eclipsed one. The existence of a kinetic barrier is also supported by the different behaviors of the vibrational spectra along the different isotherms. The Raman and IR measurements show that the spectral modifications do not occur at 30 K, are barely detectable at 150 K, and are evident at 250 K and room temperature. The barrier to the methyl group rotation is reported to be 118 K in the nitromethane crystal.[10] All of our powdered samples were prepared by pressurizing the liquid at room temperature, thus obtaining phase I crystallites, and then cooling them. It is likely that while the transition to phase II occurred along the isotherms at 250 and 300 K, at 30 K, and to some extent at 150 K, phase II was not formed because of the kinetic barrier.

Conclusions

The crystal structure of nitromethane at room temperature was found to be orthorhombic $P2_12_12_1$ with four molecules per unit cell up to the decomposition threshold pressure. The EOS was extended up to 27.3 GPa, close to the chemical instability threshold pressure. The refinement of the atomic positions allowed us to follow the changes occurring in the crystal structure that were envisaged by the pressure evolution of the vibrational spectra at room temperature. These changes consist of the blocking of the methyl group libration about the C−N bond axis. As a matter of fact, at room temperature and low pressure there is conformational disorder with respect to this libration, with two more stable orientations of the methyl with respect to the NO_2 group rotated by 50−60° from each other. This conformationally disordered phase (phase I) disappears gradually on increasing pressure if the temperature is high enough to overcome the kinetic barrier to the methyl group rotation in the crystal. This internal rearrangement is ended only at 11.0 GPa and phase II, containing only molecules with a nearly eclipsed position of the methyl group with respect to the NO_2 plane, is stabilized by a network of intermolecular O···H−C interactions built mainly in the *bc* planes. The minimum O···H distance at 15 GPa is 2.16 Å. We know that in the

high-pressure molecular conformation the relative positions and interactions in nitromethane lead to a pressure-induced chemical reaction.[11] New experiments focused on this topic are currently performed in our laboratory, and with the present work we made some steps forward in understanding the chemical transformation dynamics.

Acknowledgment. This work has been supported by the European Union under Contract RII3-CT2003-506350, by the Italian Ministero dell'Universita e della Ricerca Scientifica e Tecnologica (MURST). We thank the staff of ID09 at the ESRF and Dr. Pascal Munsch for their help with the X-ray diffraction measurements and aknowledge the ESRF for provision of synchrotron radiation facility during beamtime allocated to proposals HS-2157 and HS-2832.

References and Notes

(1) Manaa, M. R.; Reed, E. J.; Fried, L. E.; Galli, G.; Gygi, F. *J. Chem. Phys.* **2004**, *120*, 10146−10153.
(2) Winey, J. M.; Gupta, Y. M. *J. Phys. Chem. B* **1997**, *101*, 10733−10743.
(3) Bardo, R. D. In *Proceedings of the Eighth Symposyum (Int.) on Detonation*, NSWC MP 86-194; NSWC White Oak, Silver Spring, MD 20903-5000, Albuquerque, NM, July 15, 1985.
(4) Piermarini, G. J.; Block, S.; Miller, P. J. *J. Phys. Chem.* **1989**, *93*, 457−462.
(5) Courtecuisse, S.; Cansell, F.; Fabre, D.; Petitet, J. P. *J. Chem. Phys.* **1995**, *102*, 968−974.
(6) Pruzan, Ph.; Canny, B.; Power, C.; Chervin, J. C. In *Proceedings of the XVII International Conference on Raman Spectroscopy (ICORS 2000)*; Zhang, S.-L., Zhu, B.-f., Eds.; John Wiley and Sons: New York, 2000; p 142.
(7) Schettino, V.; Bini, R.; Ceppatelli, M.; Ciabini, L.; Citroni, M. *Adv. Chem. Phys.* **2005**, *131*, 105−242.
(8) Ciabini, L.; Santoro, M.; Gorelli, F. A.; Bini, R.; Schettino, V.; Raugei, S. *Nat. Mater.* **2007**, *6*, 39−43.
(9) Trevino, S. F.; Prince, E.; Hubbard, C. R. *J. Chem. Phys.* **1980**, *73*, 2996−3000.
(10) Trevino, S. F.; Rymes, W. H. *J. Chem. Phys.* **1980**, *73*, 3001−3006.
(11) Cromer, D. T.; Ryan, R. R.; Schiferl, D. *J. Phys. Chem.* **1985**, *89*, 2315−2318.
(12) Yarger, F. L.; Olinger, B. *J. Chem. Phys.* **1986**, *85*, 1534−1538.
(13) Von Dreele, R. B. *High Pressure Res.* **1995**, *14*, 13−19.
(14) Liu, H.; Zhao, J.; Wei, D.; Gong, Z. *J. Chem. Phys.* **2006**, *124*, 124501−124510.
(15) Margetis, D.; Kaxiras, E.; Elstner, M.; Frauenhim, Th.; Manaa, M. R. *J. Chem. Phys.* **2002**, *117*, 788−799.
(16) Sorescu, D. C.; Rice, B. M.; Thompson, D. L. *J. Phys. Chem. B* **2000**, *104*, 8406−8419.
(17) Reed, E. J.; Jannopulos, J. D.; Fried, L. E.; *Phys. Rev. B* **2000**, *62*, 16500−16509.
(18) Pinan-Lucarre, J-P.; Ouillon, R.; Canny, B.; Pruzan, Ph.; Ranson, P. *J. Raman Spectrosc.* **2003**, *34*, 819−825.
(19) Datchi, F.; Ninet, S.; Gauthier, M.; Saitta, M. A.; Canny, B.; Decremps, F. *Phys. Rev. B* **2006**, *73*, 174111−174115.
(20) Mao, H. K.; Bell, P. M.; Shaner, J. W.; Steinberg, D. J. *J. Appl. Phys.* **1978**, *49*, 3276−3283.
(21) Chervin, J. C.; Canny, B.; Gauthier, M.; Pruzan, Ph. *Rev. Sci. Instrum.* **1993**, *64*, 203−206.
(22) Bini, R.; Ballerini, R.; Pratesi, G.; Jodl, H. J. *Rev. Sci. Instrum.* **1997**, *68*, 3154−3160.
(23) Hammerslay, A.; Svensson, S. O.; Hanfland, M.; Fitch, A. N.; Hausermann, D. *High Pressure Res.* **1996**, *14*, 235−248.
(24) Boultif, A.; Louer, D. *J. Appl. Cryst.* **1991**, *24*, 987−993.
(25) Murnaghan, F. D. *Finite Deformation of an Elastic Solid*; Dover Publications: New York, 1951; p 73.
(26) Vinet, P.; Ferrante, J.; Rose, J. H.; Smith, J. R. *J. Geophys. Res.* **1987**, *92*, 9319−9325.
(27) Holzapfel, W. B. *High Pressure Res.* **2002 22**, 209−216.
(28) Cohen, R. E.; Gulseren, O.; Hemley, R. J. *Am. Mineral.* **2002**, *85*, 338−344.
(29) Wolanin, E.; Pruzan, Ph.; Chervin, J. C.; Canny, B.; Gauthier, M.; Hausermann, D.; Hanfland, M. *Phys. Rev. B* **1997**, *56*, 5781.
(30) Kabsch, W. J. *J. Appl. Crystallogr.* **1993**, *26*, 795−800.
(31) Sheldrick, G. M. *SHELX-97*; Dept. of Structural Chemistry, Tammannstrasse 4, 37077 Göttingen, Germany.
(32) Altomare, A.; Cascarano, G.; Giacovazzo, C.; Guagliardi, A. *J. Appl. Crystallogr.* **1993**, *26*, 343−350.
(33) Betteridge, P. W.; Carruthers, J. R.; Cooper, R. I.; Prout, K.; Watkin, D. J. *J. Appl. Crystallogr.* **2003**, *36*, 1487.
(34) Ouillon, R.; Pinan Lucarre, J. P.; Ranson, P.; Baranovic, G. *J. Chem. Phys.* **2002**, *116*, 4611−4625.
(35) McKean, D. C.; Watt, R. A. *J. Mol. Spectrosc.* **1976**, *61*, 184−202.